03,19

# Electronic band structure and thermoelectric properties of $CH_3NH_3PbI_3$, $CsSnI_3$ and $CH_3NH_3SnI_3$: *ab initio* approach

© V.P. Zhukov[1], E.V. Chulkov[2]

[1] Institute of Solid State Chemistry, Russian Academy of Sciences, Ural Branch, Yekaterinburg, Russia
[2] HSE University, Moscow, Russia

E-mail: Zhukov@ihim.uran.ru

*Received August 30, 2023*
*Revised August 30, 2023*
*Accepted September 14, 2023*

Theoretical modeling „from the first principles“ of the electronic band structure and thermoelectric properties of iodides $CH_3NH_3PbI_3$, $CsSnI_3$ and $CH_3NH_3SnI_3$ has been performed. The simulation method is based on the electron density functional theory, the theory of electron-phonon interaction, the Boltzmann–Onsager theory of thermoelectric properties, and the Slack method for calculating phonon thermal conductivity. For a wide range of carrier concentration, the temperature dependences of conductivity, Seebeck coefficient, thermal conductivity coefficient, power function, and thermoelectric figure of merit are calculated. The calculated values of the figure of merit indicate the possibility of obtaining thermoelectrics with higher efficiency based on such compounds. It is shown that the most promising for use as a thermoelectric material is the $CsSnI_3$ compound.

**Keywords:** electronic band structure, PAW method, theory of Boltzmann, transport properties, Pb and Sn halides, methilammonium ion.

DOI: 10.61011/PSS.2023.11.57313.191

## 1. Introduction

Lead and tin trihalides, i.e. compounds of the $DMG_3$ form, where $D$ being a doping ion with charge $+1$, most often it is a methyl ammonium ion $(CH_3CN_3)^{1+}$ or a cesium ion, $M = Pb$ or Sn, and $G = Cl$, Br or I, are being intensively studied due to the prospects of their use as efficient materials in solar cells, see reviews [1–4]. The attention of researchers is also attracted by their thermoelectric properties [5–17]. In [16], polycrystalline films of the $CH_3NH_3SnI_3$ compound (hereinafter referred to as $CH_3CN_3 = MA$) were synthesized, their conductivity and Seebeck coefficient were measured, and the thermoelectric power factor was estimated. In [11], films of the $MAPbI_{3-x}Cl_x$ group of compounds were synthesized, their thermoelectric properties (TEP) were studied: conductivity, Seebeck coefficient, and thermal conductivity, power factor, and thermoelectric figure of merit. A number of theoretical studies of the properties of such compounds have also been carried out using computational methods of electron density functional theory (DFT) [7,12,13,15,18,19]. Thus, in [12] the characteristics of the band structure, TEP and mechanical properties of the $MAPbI_3$ compound were assessed, its power factor and figure of merit were calculated, and in [13], TEP and optical properties were assessed. For this compound, in [14] TEP were modeled in the dark and under light. In [6], TEP, power and figure of merit functions were calculated for $MAPbI_3$ on the basis of the Boltzmann–Onsager theory and computational methods of the DFT theory. It was predicted that at temperatures above 500 K, the figure of merit could probably be higher than 1.5, which is inherent with the most efficient semiconductor thermoelectrics. Also, high values of the figure of merit, up to 0.9 at high temperatures, were predicted for this compound in [13]. However, such predictions are cause for concern because they were obtained using outdated software based on approximations that are not entirely justified, for example, the approximation of a fixed electron-phonon relaxation time [20].

Recently, more attention has been paid to the study of tin halides, which, due to the absence of lead, have a less harmful effect on the environment. In [9,21,22], TEP of the $MASnI_3$ compound were studied in the temperature range from 325 to 350 K [9] and from 10 to 300 K [22]. It was shown that with the chosen synthesis methods, the conductivity is of the hole nature. In [9], based on thermoelectric measurements for the carrier concentration of the order of $10^{23}$ cm$^{-3}$, the power factor was estimated depending on the details of the synthesis. In [23], it was shown that at a low concentration of carriers, of the order of $10^{14}$, and a temperature from 10 to 300 K, the conductivity is of electronic nature with a very low figure of merit, from $10^{-13}$ to $10^{-7}$. A number of studies have also been carried out focused on the thermoelectric properties of the $CsSnI_3$ compound doped with various elements — see review [5] and [24], which showed that almost all the materials at temperatures up to 500 K have hole conductivity with a figure of merit not higher than 0.14. However, the number of theoretical studies devoted to tin

halides is small [17,25–28], and it is unclear whether the optimistic predictions of [7,13] are valid for this class of compounds. In particular, in [6,13,26–28] the dubious approximation of a fixed relaxation time was also used to estimate the figure of merit.

The prospect of creating highly efficient photovoltaics that are both good thermoelectrics and environmentally inert looks very attractive. The disadvantage of the available experimental data sets on TEP is that they often refer to temperatures below 400 K and do not show the dependence of TEP on carrier concentration, i.e. they are of little use for searching for dopant concentrations corresponding to the optimal values of the power and figure of merit functions. In this context, we have carried out modeling of the thermoelectric properties of a number of lead and tin compounds in a wide range of temperatures and carrier concentrations using new software based on the DFT theory [29]. The $MAPbI_3$, $CsSnI_3$ and $MASnI_3$ iodides, which were most fully studied experimentally, were chosen as objects of the study. It is known, in particular, that they have a decomposition temperature of 600, 750, and 600 K, respectively [30,31]. The modeling made it possible to evaluate the prospects for using such compounds as thermoelectrics, to clarify the role of doping ions in the formation of thermoelectric properties, to clarify the nature of the effect of temperature changes in their structure on the properties and the causes for the differences between experimental and theoretical data.

## 2. Method for calculating the band structure and thermoelectric properties

Probably the most promising method for modeling thermoelectric properties is the AMSET software package [29], which is an add-on to the VASP package [32], which implements the method of projected augmented waves (PAW) of the electron density functional theory. The calculation method implemented in AMSET is based on the Boltzmann–Onsager theory of thermoelectric properties, described both in a number of textbooks [33,34] and in previous publications devoted to TEP calculation methods [20,35,36]. The characteristics of electron transport in crystals can be obtained using the spectral conductivity function $\Sigma_{\alpha\beta}$, which is calculated on the basis of the relaxation time approximation as

$$\Sigma_{\alpha\beta}(\varepsilon) = \Sigma_n \int \frac{d\mathbf{k}}{8\pi^3} \boldsymbol{\nu}_{n\mathbf{k},\alpha} \boldsymbol{\nu}_{n\mathbf{k},\beta} \tau_{n\mathbf{k}} \delta(\varepsilon - \varepsilon_{n\mathbf{k}}), \qquad (1)$$

where $\alpha$ and $\beta$ are Cartesian coordinates $(x, y, z)$, $\varepsilon_{n\mathbf{k}}$ and $\boldsymbol{\nu}_{nk,\alpha}$ are energy and group velocity of the band state with number $n$ and wave vector $\mathbf{k}$, and $\tau_{n\mathbf{k}}$ is the corresponding relaxation time of the band state. In the Boltzmann–Onsager theory, auxiliary functions $\mathscr{L}^N_{\alpha\beta}$ depending on $\Sigma_{\alpha\beta}$ are defined:

$$\mathscr{L}^N_{\alpha\beta} = \frac{e^2}{4k_\mathrm{B}T} \int \Sigma_{\alpha\beta} \left[\cosh\left(\frac{\varepsilon - \varepsilon_\mathrm{F}}{2k_\mathrm{B}T}\right)\right]^{-2} (\varepsilon - \varepsilon_\mathrm{F})^N d\varepsilon, \quad (2)$$

where $e$ is electron charge, and $k_\mathrm{B}$ is the Boltzmann constant. It follows from the form of the $[\cosh[(\varepsilon - \varepsilon_\mathrm{F})/(2k_\mathrm{B}T)]]^{-2}$ expression that these functions depend mainly on band states near the Fermi level $\varepsilon_\mathrm{F}$. Then using $\mathscr{L}^N_{\alpha\beta}$ the following electron transport coefficients can be obtained:

$$\sigma_{\alpha\beta} = \mathscr{L}^0_{\alpha\beta}, \qquad (3)$$

$$S_{\alpha\beta} = \frac{1}{|e|^2 T} \frac{\mathscr{L}^1_{\alpha\beta}}{\mathscr{L}^0_{\alpha\beta}}, \qquad (4)$$

$$\kappa_{\alpha\beta} = \frac{1}{|e|^2 T} \frac{\mathscr{L}^1_{\alpha\beta}}{\mathscr{L}^0_{\alpha\beta}} \left[\frac{(\mathscr{L}^1_{\alpha\beta})^2}{\mathscr{L}^0_{\alpha\beta}} - \mathscr{L}^2_{\alpha\beta}\right]. \qquad (5)$$

Here $\sigma_{\alpha\beta}$ is specific conductivity, $S_{\alpha\beta}$ is Seebeck coefficient, and $\kappa_{\alpha\beta}$ is electronic contribution to the thermal conductivity. It is known that a significant contribution to the thermal conductivity comes from the phonon subsystem. This contribution, $k_\mathrm{phon}$, must be calculated separately, and then the total thermal conductivity can be calculated as

$$k_\mathrm{tot} = k_\mathrm{el} + k_\mathrm{phon}. \qquad (6)$$

Here it is assumed that the values are averaged over Cartesian coordinates.

The main problem, the accuracy and time of calculations depends on, is the calculation of the electron relaxation time $\tau_{n\mathbf{k}}$. It is assumed that Matthiessen's rule is valid, according to which the relaxation rate is calculated as

$$1/\tau_{n\mathbf{k}} = \Sigma_m 1/\tau^m_{n\mathbf{k}}, \qquad (7)$$

where $\tau^m_{n\mathbf{k}}$ are contributions from various electron scattering mechanisms. The AMSET software package implements the most complete, although not comprehensive, set of methods for calculating relaxation times. Namely, these are calculations of the time of inelastic relaxation of electrons on acoustic and optical phonons, elastic piezoelectric relaxation on phonons and elastic relaxation on point defects — see [29]. At the same time, a number of approximations are used that significantly speed up calculations in comparison with previous methods [20,35,36]. In our case, effective are the use of the Christoffel method in calculations of scattering on acoustic phonons [37] and the Fröhlich method in calculations of scattering on optical phonons. The Christoffel method requires the calculation of a complete set of elastic constants, and the Fröhlich method requires the calculation of the deformation potentials of band states in the presence of phonons and dielectric constants of the crystal, which can be done using the PAW method implemented in the VASP software package. The calculation procedure is described in [29].

In the calculations of the band structure using the VASP method, we represented wave functions and electron density in the form of an expansion in plane waves with an energy of up to 300 eV and for 170 wave vectors in the irreducible part of the Brillouin zone. Self-consistency of the energy of band states was carried out with an accuracy of $10^{-8}$ eV. Due to the fact that TEP calculations require the calculation of elastic constants and deformation potentials, the crystal structure was relaxed in accordance with the forces acting on the atoms. The relaxation process was considered complete when the variations in the total cell energy at the last five relaxation steps did not exceed $10^{-5}$ eV. A functional of the PBEsol type [38] was used as an exchange-correlation functional.

When calculating TEP, contributions during the relaxation of band states from their interaction with acoustic and optical phonons were taken into account. Calculations of elastic scattering on oxygen vacancies with charge +2 were also carried out using the method implemented in AMSET, proposed by Brooks and Herring [34]. It was shown that with the concentrations of current carriers under consideration, in this case holes, the contributions of such scattering to the relaxation rate $1/\tau_{n\mathbf{k}}$ are negligible in comparison with the contributions of other scattering mechanisms.

The AMSET software package provides for refinement of calculations of the band structure near the Fermi level by interpolating the results over a dense grid of wave vectors using the method described in [20]. We provided a 40-fold compaction of the set of wave vectors along each coordinate, i. e. transition to 1088000 wave vectors in the irreducible part of the Brillouin zone.

The only experimental parameter in the calculations is the band gap. For $MAPbI_3$, the experimental value of $E_g^{\text{exper}}(MAPbI_3) = 1.5$ eV [39] was adopted. For other compounds, due to uncertainties in the experimental data, the band gap was calculated according to the following rule:

$$E_g(\text{comp}) = E_g^{\text{exper}}(MAPbI_3)E_g^{\text{calc}}(\text{comp})/E_g^{\text{calc}}(MAPbI_3),$$

where $E_g^{\text{calc}}(\text{comp})$ being band gap of the „comp“ compound from the calculations with relaxation of the crystal structure.

In the thermal conductivity calculations, a major problem is the calculation of the phonon subsystem contribution. The method for „*ab initio*“ calculating the phonon part of thermal conductivity is implemented in the Phono3py software package, compatible with the VASP computational method. However, the duration of such calculations is so long that they are feasible for structures with only a few atoms per cell. Therefore, we used a model approach developed by Slack [40–44] and based on the Debye approximation for phonon states of acoustic modes. The physical basis of the approach is presented in [44], and the method of *ab initio* calculations on this basis is demonstrated in [45]. In [42], it was shown that at a temperature not very different from the Debye temperature the phonon thermal conductivity can be represented in the following form:

$$k_{\text{phon}} = A\frac{M_a\theta^3\delta^3 n_{\text{pr}}^{1/3}}{\gamma^2 T}. \tag{8}$$

Here $M_a$ is average atomic mass, $\theta$ is the Debye temperature, $\delta^3$ is average atomic volume, $n_{\text{pr}}$ is number of atoms in a primitive cell, $\gamma$ is Grüneisen parameter, $T$ is temperature. The $A$ constant was defined in [46]:

$$A = \frac{2.43\cdot 10^{-8}}{1 - 0.514/\gamma + 0.228/\gamma^2}. \tag{9}$$

The acoustic Debye temperature can be expressed in terms of the sound velocity $v$ in the form [47]:

$$\theta = \frac{h}{k_{\text{B}}}\left[\frac{3n_c}{4\pi V_c}\right]^{1/3} v n_{\text{pr}}^{-1/3}, \tag{10}$$

where $h$ is Planck's constant, $k_{\text{B}}$ is Boltzmann's constant, $n_c$ is number of atoms in the cell, $V_c$ is volume of the cell. The sound velocity can be obtained *ab initio* using its expression in terms of the bulk modulus of elasticity $B$ and the shear modulus $G$. The form of these expressions for longitudinal and transverse acoustic waves is as follows [45]:

$$v_L = \sqrt{\frac{B + 4/(3G)}{\rho}}, \quad v_s = \sqrt{\frac{G}{\rho}}, \tag{11}$$

where $\rho$ is compound density, and averaging can be performed according to the following rule:

$$v = \left[\frac{1}{3}\left(\frac{1}{v_L^3} + \frac{2}{v_s^3}\right)\right]^{-1/3}. \tag{12}$$

The moduli $B, G$ are calculated from the complete set of elastic constants. For a number of structures, including simple cubic ones, the corresponding relations are given in [48]. The Grüneisen parameter in equations (9) and (10) can be obtained if the Poisson modulus $\Pi$ is known:

$$\gamma = \frac{3}{2}\left(\frac{1+\Pi}{2-3\Pi}\right), \tag{13}$$

which, in turn, can be obtained if the velocities of longitudinal $v_L$ and transverse $v_s$ acoustic modes are known

$$\Pi = \frac{1 - 2(v_s/v_L)^2}{2 - 2(v_s/v_L)^2}. \tag{14}$$

To obtain elastic constants with high accuracy, the number of plane waves used in the charge density representation in the VASP code was increased eightfold in our calculations. In addition, due to the fact that localized states of the methylammonium ion do not contribute to acoustic phonons, the atoms of this ion were omitted in the calculations of $N$ and $M_a$.

Based on the calculated values of conductivity, Seebeck coefficient, and thermal conductivity coefficient, we calculated the thermoelectric power function

$$P = S^2\sigma \tag{15}$$

and figure of merit

$$ZT = \frac{S^2\sigma}{k_{\text{tot}}}\,T. \tag{16}$$

## 3. Band structure of $MAPbI_3$, $CsSnI_3$, $MASnI_3$ compounds

Figure 1 shows a lattice cell of a simple cubic structure, typical for compounds doped with the MA ion at temperatures above 500 K. It was assumed that the C–N-bond is directed along the $a$ axis, although it is known from experiments that the direction of this bond is disoriented [49]. Due to the relaxation in the process of calculation, the structure acquires an orthorhombic distortion with periods along $a, b, c$ axes equal to 6.20, 6.15, and 6.14 Å instead of 6.27 Å for a simple cubic structure. In the following, we will show that neglecting the disorientation does not lead to a noticeable deterioration in the results of thermoelectric properties calculations.

Figure 2 shows the total and partial densities of states (DoS) for $MAPbI_3$. The basis of atomic orbitals here includes 6*s*- and 6*p*-orbitals of lead, 5*s*- and 5*p*-orbitals of iodine and valence orbitals of nitrogen and carbon. The 5*s*-orbitals of iodine are responsible for the formation of a group of band states near −12 eV, and the 5*p* states of iodine are responsible for the group from −4 eV to the Fermi level. The 6*s*-lead orbitals form a group of band states around −8 eV, which have noticeable dispersion, and are also included in the group from −4 eV to the Fermi level. It follows from the presence of dispersion and mixing of lead and iodine DoSs that their orbitals are hybridized and form a framework of chemical bonds in

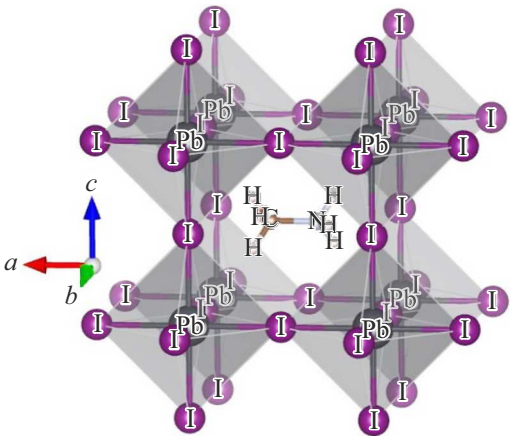


**Figure 1.** Lattice cell of a simple cubic structure of $MAPbI_3$, $MASnI_3$.

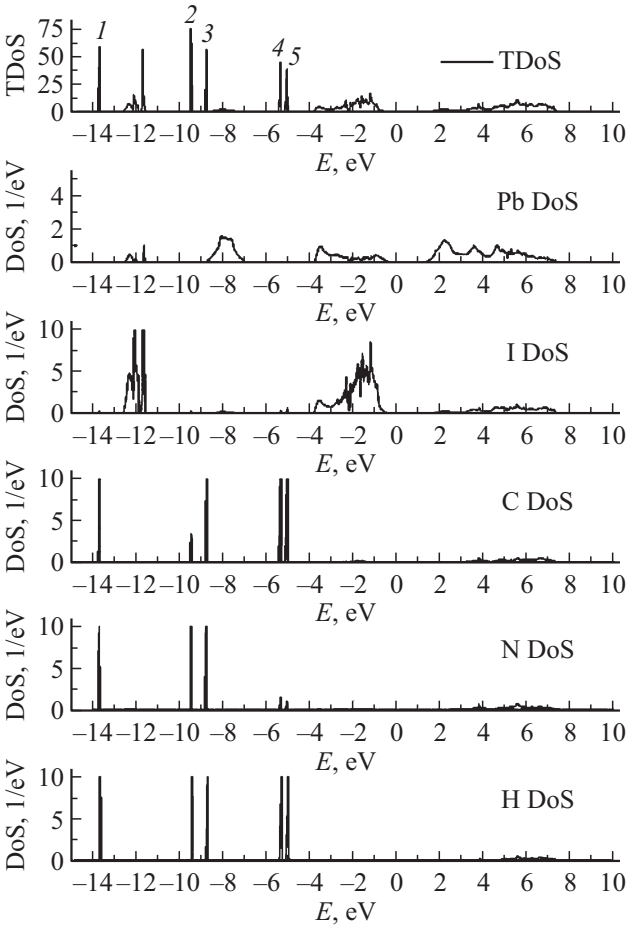


**Figure 2.** Total (per lattice cell) and partial densities of states (DS), calculated per 1 atom, for $MAPbI_3$. The Fermi level is taken as zero energy, equal to the top of the valence band in this case.

octahedra of $PbI_6$. Band states with almost no dispersion, marked on the complete DoS with numbers from *1* to *5*, belong to carbon, nitrogen, and hydrogen atoms. They are hybridized with each other but not with the orbitals of lead and iodine, i. e. they correspond to the molecular orbitals of the methylammonium ion. The localized nature of the states of the MA ion is confirmed by the form of isosurfaces of the wave functions for the Γ-point shown in Figure 3. When the wave function value is $4 \cdot 10^{-6}$ Å$^{-3}$, there are no contributions from lead and iodine; their small contributions to the isosurface are manifested when the wave function is 10 times smaller. This means that the electron density outside the isosurfaces shown in Figure 3 is almost 100 times less than inside them, i. e. the bond between the octahedra $PbI_6$ and the MA ion is weak. In the following, we will consider the consequences of this effect for the thermoelectric properties.

For the $CsSnI_3$ compound with a perovskite structure, where a cesium ion is present instead of the MA ion (Figure 4), the calculation results are shown in Figure 5.

Calculations were carried out with the basis of 5*s*-, 5*p*-orbitals of tin and iodine atoms and the extended set

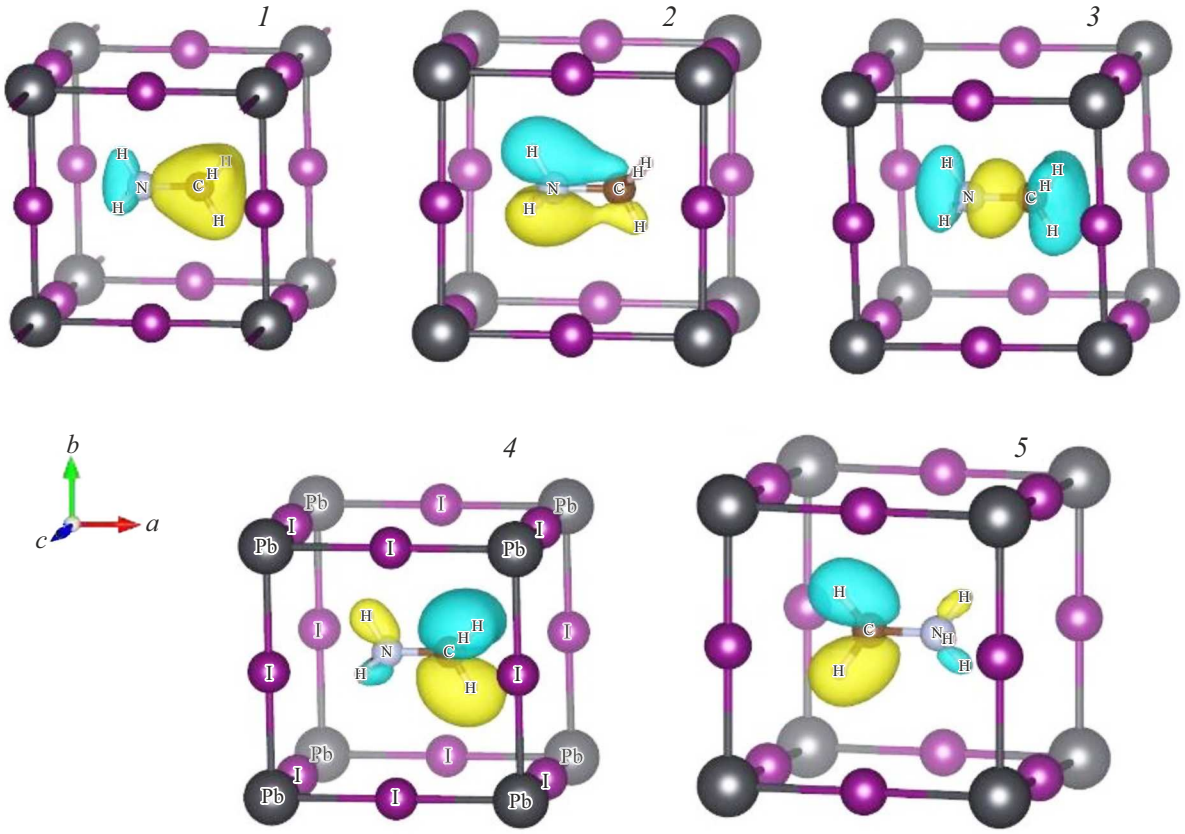


**Figure 3.** Isosurfaces of wave functions at the Γ-point of localized states of the MA ion in $CH_3NH_3SnI_3$. Calculated for values on isosurfaces equal to $4 \cdot 10^{-6}$ units $Å^{-1}$ (yellow lobes) and $-4 \cdot 10^{-6}$ (blue lobes) units $Å^{-3}$.

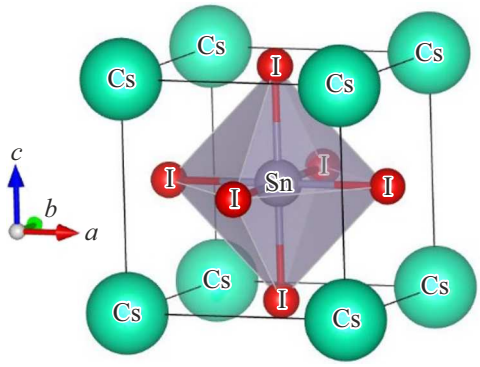


**Figure 4.** Lattice cell of $CsSnI_3$.

of 5*s*-, 5*p*-, 6*s*-orbitals of cesium atoms. Band states near −12.5 eV are formed from 5*s*-orbitals of iodine atoms and small impurities of 5*s*-orbitals of tin. Near −9 eV there is a peak of dispersionless states formed from 5*s*- and 5*p*-orbitals of cesium atoms. In the energy range from −8.2 to −6.2 eV, there is a band composed mainly from 5*s*-orbitals of tin atoms, which are hybridized with 5*s*-orbitals of iodine atoms. In the range from −4.4 to −1.1 eV, there are band states formed from 5*p*-orbitals of iodine and 5*p*-orbitals of tin, and above this band, up to the Fermi level, there are unhybridized bands of 5*p*-orbitals of iodine.

Figure 6 shows the total and partial DoSs of the $MASnI_3$ compound.

In general terms, the band structure of $MASnCl_3$ is similar to the structure of $MAPbI_3$: similar types of hybrid and localized states are present.

## 4. Thermoelectric properties of $MAPbI_3$, $CsSnI_3$, $MASnI_3$compounds

The results of our *ab initio* calculations of TEP and the power function in the temperature range from room temperature to $T$ of about 600 and 750 K, i. e. decomposition temperatures of compounds, are shown in Figures 7−10 for a wide range of hole concentrations.

It can be seen that changes in TEP with an increase in both temperature and hole concentration $n_h$ for all compounds differ very little. As the temperature increases, a significant decrease in the Seebeck coefficient is observed, while the conductivity increases by several orders of magnitude. These trends have opposite effects on the power function $P = S^2\sigma$, but at all temperatures $P$ increases with increasing $n_h$, although the details of the change in $P$ for

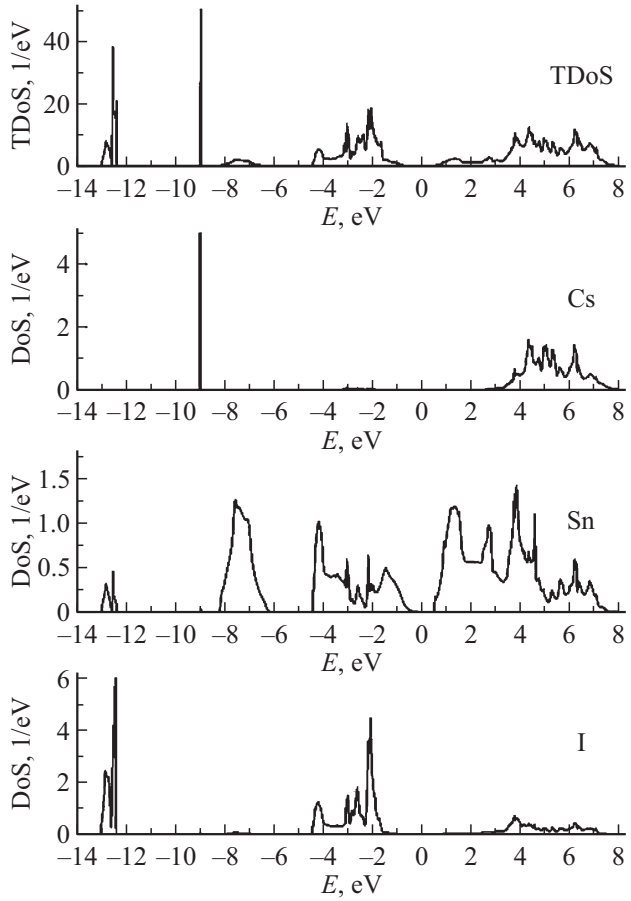


**Figure 5.** Total and partial densities of states of $CsSnI_3$.

different compounds differ due to subtle details of the change in $S$ and $\sigma$. The calculated values of $P$ turn out to be significantly higher than the experimental ones, $0.03\,\mathrm{mW/(m\cdot K^2)}$ for $MaPbI_3$ [13] and $0.13\,\mathrm{mW/(m\cdot K^2)}$ for $CsSnI_3$ [5]. The results of calculations of the dependences of the figure of merit $ZT$ on temperature are shown in Figure 11; they reach a value of $\sim 1$ comparable to the figure of merit values for the most efficient thermoelectrics, $\sim 2$ [50]. The dependences of $ZT$ on the hole concentration at different temperatures are almost the same; Figure 12 shows them as examples for a temperature of 300 K. It can be seen that for all compounds the maximum ZT is achieved at the optimal carrier concentration of $\sim 10^{18}\,\mathrm{cm^{-3}}$. It should be noted that the extreme form of the dependences of figure of merit on concentration occurs for a fairly wide class of thermoelectrics [51,52].

Figure 13 shows the temperature dependences of the total thermal conductivity coefficient $k_{\mathrm{tot}}$ and its terms, i. e. electronic $k_{\mathrm{el}}$ and phonon $k_{\mathrm{phon}}$ contributions calculated using the Slack model. It can be seen that the dominant contribution determining the value of $k_{\mathrm{tot}}$ is the phonon contribution, as is the case for other classes of thermoelectrics [53–55]. The results are in reasonable agreement with the data obtained for $MaPbI_3$ [6] from the *ab initio* approach implemented in the Phono3py software package [56]: both the low value of thermal conductivity, $\sim 0.5$ at 300 K, and its temperature decrease are reproduced.

It is noteworthy that both the TEP graphs and the values of $P$ and $ZT$ for $CsSnI_3$ and $MASnI_3$ are almost the same. Due to the lack of the problem of doping ion orientation relative to the crystallographic axes for $CsSnI_3$, it follows that for $MASnI_3$, and probably for $MAPbI_3$, the orientation of the ion $MA = (CH_3CN_3)^{1+}$ affects the thermoelectric properties negligibly, as do small deviations of the crystal symmetry from the cubic one. That is, the role of the MA ion in the formation of TEP consists mainly in the introduction of electrons into the $PbI_3$, $SnI_3$ subsystems, which determines the emergence of semiconductor properties. It should be noted that this result contradicts the conclusions of [57] about the effect of the MA ion orientation, made without TEP modeling only on the basis of analysis of changes in the band structure with varying orientation.

It can be seen from the consideration of the graphs of $ZT$ for the hole concentration of $n_h = 10^{18}\,\mathrm{cm^{-3}}$ that at temperatures above room temperature, within the limits of structure stability, the calculated value of $ZT$ for $MaPbI_3$ is

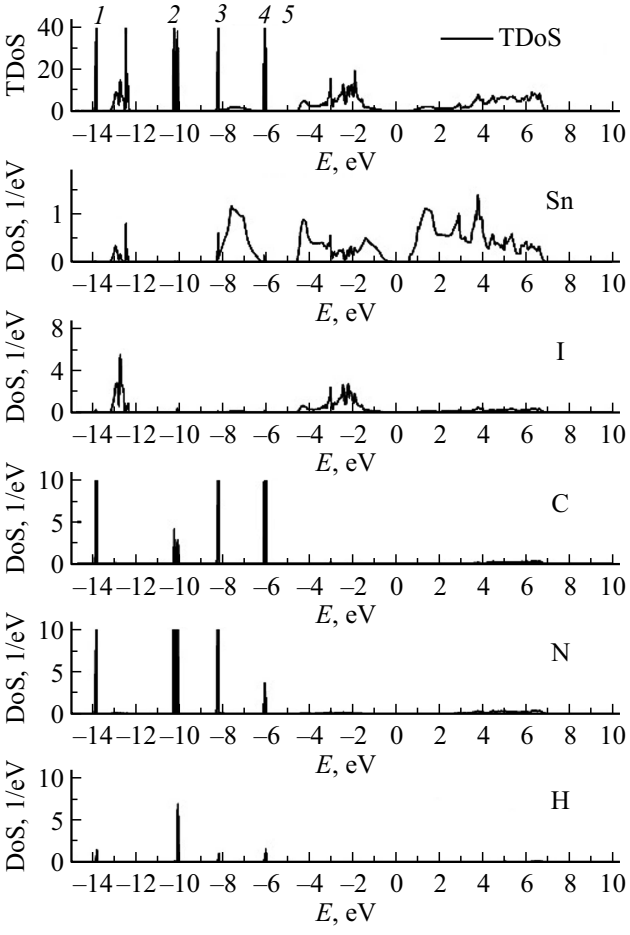


**Figure 6.** Total and partial DoS of the $MaSnI_3$ compound. DoSs are given in 1/eV.

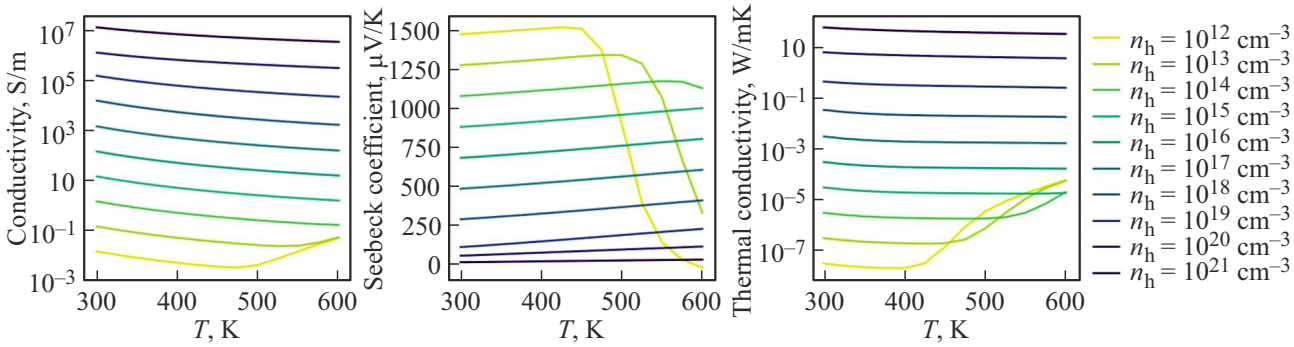


**Figure 7.** Calculated values of thermoelectric properties of the $MAPbI_3$ compound.

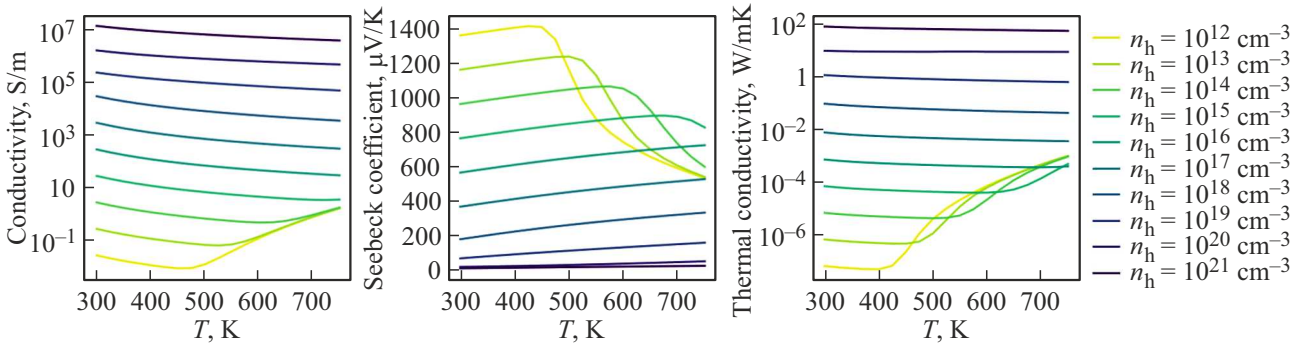


**Figure 8.** Calculated values of thermoelectric properties of the $CsSnI_3$ compound.

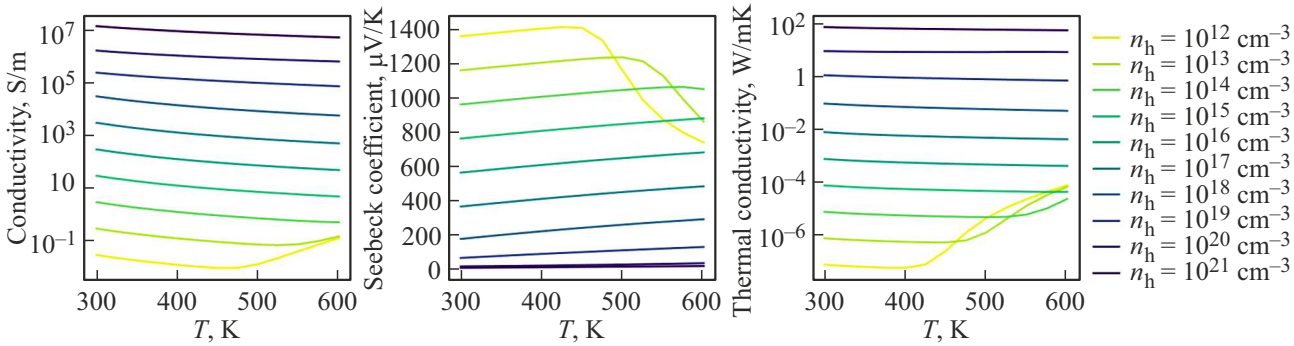


**Figure 9.** Calculated values of thermoelectric properties of the $MASnI_3$ compound.

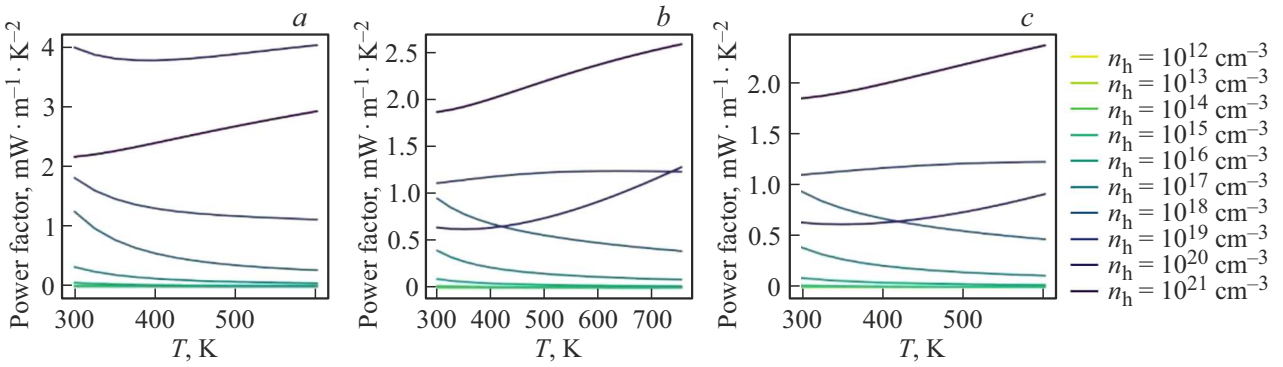


**Figure 10.** Calculated values of the power function for $MAPbI_3$ (*a*), $CsSnI_3$ (*b*), $MASnI_3$ (*c*).

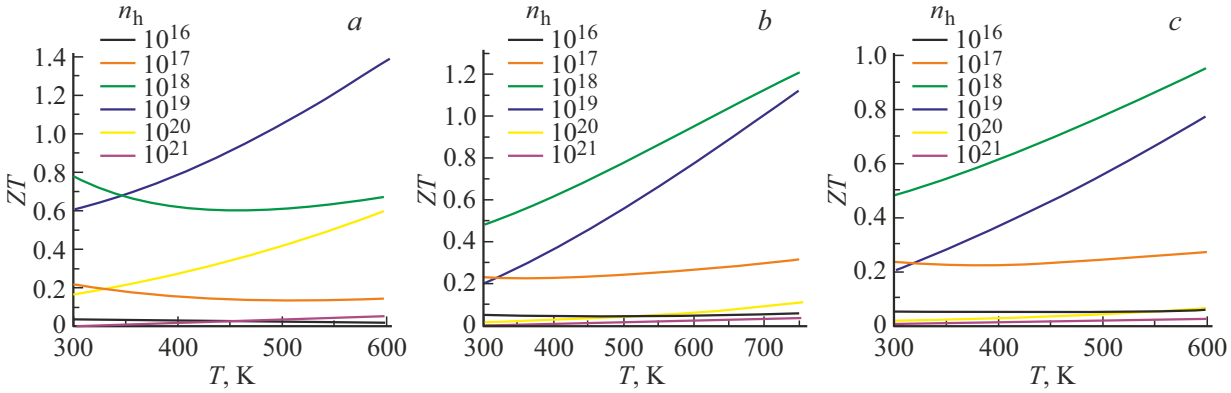


**Figure 11.** Calculated values of thermoelectric figure of merit $ZT$ for compounds of $CH_3NH_3SnI_3$ ($a$), $CsSnI_3$ ($b$), $CH_3NN_3SnI_3$ ($c$).

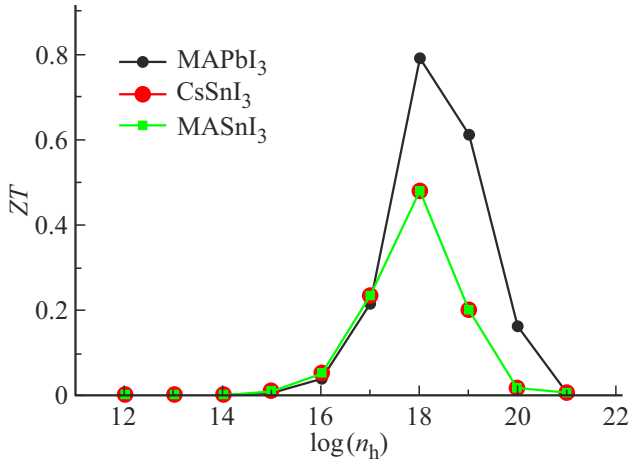


**Figure 12.** Calculated values of the figure of merit $ZT$ depending on the hole concentration for compounds of $CH_3NH_3SnI_3$, $CsSnI_3$ and $CH_3NH_3SnI_3$ at a temperature of 300 K.

at a level of 0.6. For $CsSnI_3$ and $MASnI_3$ (the results differ very little) this value increases to the level of 1.1, i.e. the calculations predict higher efficiency for these compounds. The calculated values of conductivity, power and figure of merit functions significantly exceed the experimentally obtained values [9,16,18,22,23]. One of the causes for it is that the modeling refers to a bulk single crystal, whereas the experimental data is usually obtained for polycrystals or nanostructures. The higher values of conductivity, and therefore the higher values of $P$ and $ZT$, are explained by the fact that its calculations do not take into account the contribution during relaxation from the scattering of current carriers that occurs at grain boundaries. Modeling such scattering is still an unsolved problem in the theory of thermoelectric properties.

However, it can be shown that for thermoelectrics with methylammonium ion there is also another cause for the low experimental values of $P$ and $ZT$. One of the advantages of the Boltzmann–Onsager theory is the ability to calculate the Seebeck coefficient on its basis with a fairly high accuracy. It follows from equation (4) that a mutual reduction in the relaxation time included in both the numerator and the denominator can be expected, and, consequently, the insensitivity of the calculation results to the relaxation time, which determines the high accuracy. Good agreement of the Seebeck coefficient values with experiment for a large number of compounds is confirmed

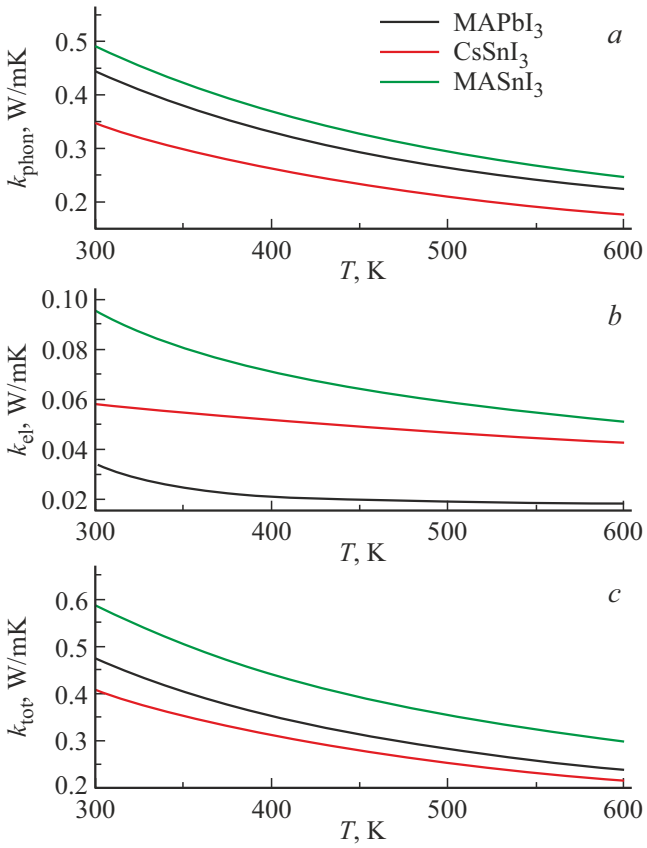


**Figure 13.** Calculated dependences of the thermal conductivity coefficients of the compounds of $CH_3NH_3SnI_3$, $CsSnI_3$ and $CH_3NH_3SnI_3$ at a carrier concentration of $10^{18}$ cm$^{-3}$. Here $k_{phon}$, $k_{el}$ and $k_{tot}$ are, respectively, the phonon contribution, the electronic contribution and the total thermal conductivity.

by literature data [29,52], i.e. if the carrier concentration is unknown, then calculations of the Seebeck coefficient can be used to estimate it. For $MASnI_3$ and $MAPbI_3$ in [9,22,58] in the temperature range from 300 to 400 K, very low values of the Seebeck coefficient were obtained, from 5 to 100 $\mu$V/K, but without indicating the carrier concentration. According to our estimates of the Seebeck coefficient, Figures 8–10, this should correspond to a hole concentration from $10^{20}$ to $10^{21}$ cm$^{-3}$, i.e. from $\sim 0.025$ to $\sim 0.25$ holes per cell. The explanation is that during the process of synthesis, apparently, non-stoichiometric compounds of the $(CH_3NH_3)_{1-x}Sn(Pb)I_3$ type were formed, where $x \approx 0.025-0.25$, i.e. with a deficiency of methylammonium ion. This is consistent with the idea that the electronic states of the methylammonium ion are localized, i.e. this ion is weakly bound to the rest of the crystal structure and can be easily removed from it. This can be confirmed by the results of [59], showing that a small decrease in weight upon heating the $MAPbI_3$ begins at 500 K, i.e. noticeably below the decomposition temperature. Based on calorimetric measurements, it was also shown in [60] that $MAPbI_3$ is thermodynamically unstable, along with similar compounds with chlorine and bromine.

## 5. Conclusion

Previously performed experimental studies of lead and tin trihalides, which have hole conductivity when methylammonium or cesium ions are implanted in their structure, previously led to the conclusions about very modest prospects for using their thermoelectric properties, because studies at temperatures below 100°C showed low figures of merit. However, theoretical estimates of the figure of merit previously carried out for the $MAPbI_3$ compound showed that for $MAPbI_3$ single crystals at higher temperatures much higher values of the figure of merit can be expected. Using a more advanced theoretical approach, we concluded that high figures of merit can be expected for all three compounds considered, i.e. $MAPbI_3$, $CsSnI_3$, and $MASnI_3$. However, the analysis of the electronic structure of $MAPb(Sn)I_3$ compounds shows a weak bond between the MA ion and the framework of interconnected octahedra of $PbI_6$, i.e. the possibility of easy removal of the MA ion with a corresponding decrease in the Seebeck coefficient. Due to the fact that the $CsSnI_3$ compound is free from such a defect and has the highest decomposition temperature, it appears to be probably the most promising thermoelectric of all the compounds considered.

### Funding

The study has been funded by the state budget. Calculations were performed at the URAN cluster of the Mathematics and Mechanics Institute of the Ural Branch of RAS.

### Conflict of interest

The authors declare that they have no conflict of interest.

## References

[1] M.A. Green, A. Ho-Baillie, H.J. Snaith. Nature Photonics **8**, *7*, 506 (2014).
[2] H. Li, F. Li, Zh. Shen, S.-T. Han, J. Chen, Ch. Dong, Ch. Chen, Y. Zhou, M. Wang. Nano Today **37**, 101062 (2021).
[3] M. Dawson, C. Ribeiro, M.R. Morelli. Mater. Res. **25**, *7*, e20210441 (2022).
[4] Sb. tez. dokl. I Mosk. osenney mezhdunar. konf. po perovskitnoy fotovoltaike (MAPPIC 2019). KDU, Dobrosvet, M., (2019), 51 s. (in Russian).
[5] A.K. Baranwal, A. Kumar, Sh. Hayase. Nanomater. **12**, *22*, 4055 (2022).
[6] A. Filippetti, C. Caddeo, P. Delugas, A. Mattoni. J. Phys. Chem. C **120**, *50*, 28472 (2016).
[7] S. Choudhary, A. Shukla, J. Chaudhary, A.S. Verma. Int. J. Energy. Res. **44**, *14*, 11614 (2020).
[8] S. Saini, A.K. Baranwal, T. Yabuki, S. Hayase, K. Miyazaki. J. Electron. Mater. **49**, *5*, 2890 (2020).
[9] Q. Wang, Y. Tang, Z. Horita, S. Iikubo. Mater. Res. Lett. **10**, *8*, 521 (2022).
[10] I.O.A. Ali, D.P. Joubert, M.S.H. Suleiman. Eur. Phys. J. B **91**, *9*, 263 (2018).
[11] A.M.M.T. Karim, M.K.R. Khan, M.S. Hossain. ACS Omega **6**, *26*, 16775 (2021).
[12] A. Kore, H. Murari, P. Singh. J. Phys. D **54**, *30*, 305503 (2021).
[13] A. Shukla, V.K. Sharma, S.K. Gupta, A.S. Verma. Mater. Res. Express **6**, *12*, 126323 (2020).
[14] P. Wu, Y. Xiong, L. Sun, G. Xie, L. Xu. Organic Electron. **55**, 90 (2018).
[15] H. Xie, S. Hao, J. Bao, T.J. Slade, G.J. Snyder, C. Wolverton, M.G. Kanatzidis. J. Am. Chem. Soc. **142**, *20*, 9553 (2020).
[16] T. Ye, X. Wang, X. Li, A.Q. Yan, S. Ramakrishna, J. Xu. J. Mater. Chem. C **5**, *5*, 1255 (2017).
[17] L. Yu, W. Kassem, R. Bude, L. Divay, J. Amrit, S. Volz. 21st Int. Workshop on Thermal Investigations of ICs and Systems (THERMINIC) B, 1 (2015).
[18] E. Menéndez-Proupin, P. Palacios, P. Wahnón, J.C. Conesa. Phys. Rev. B **90**, *4*, 045207 (2014).
[19] P. Umari, E. Mosconi, F. De Angelis. Sci. Rep. **4**, *1*, 4467 (2013).
[20] G.K.H. Madsen, D.J. Singh. Comp.Phys. Commun. **175**, *1*, 67 (2006).
[21] S. Saini, I. Matsumoto, S. Kishishita, A.K. Baranwal, T. Yabuki, S. Hayase, K. Miyazaki. Jpn J. Appl. Phys. **61**, SE1019 (2022).
[22] Y. Takahashi, R. Obara, Z.-Z. Lin, Y. Takahashi, T. Naito, T. Inabe, S. Ishibashi, K. Terakura. Dalton Trans. **40**, *20*, 5563 (2011).
[23] X. Mettan, R. Pisoni, P. Matus, A. Pisoni, J. Jacimović, B. Náfrádi, M. Spina, D. Pavuna, L. Forró, E. Horváth. J. Phys. Chem. C **119**, *21*, 11506 (2015).
[24] S. Yu, F. Qian, M. Hu, Z. Ge, J. Feng, X. Chong. Mater. Lett. **308**, *Part A*, 131127 (2022).
[25] T. Das, G. Di Liberto, G. Pacchioni. J. Phys. Chem. C **126**, *4*, 2184 (2022).

[26] Z.-Q. Ma, H. Pan, P.K. Wong. J. Electron. Mater. **45**, *11*, 5956 (2016).
[27] T. Shi, H. Zhang, W. Meng, Q. Teng, M. Liu, X. Yang, Y. Yan, H.-L. Yip, Y.-J. Zhao. J. Mater. Chem. A **5**, *29*, 15124 (2017).
[28] Y.S. Wudil, Q. Peng, A.Q. Alsayoud, M.A. Gondal. Comput. Mater. Sci. **201**, 110917 (2022).
[29] A.M. Ganose, J. Park, A. Faghaninia, R. Woods-Robinson, K.A. Persson, A. Jain. Nature Commun. **12**, *1*, 2222 (2021).
[30] M. Zhang, K. Chen, Y. Wei, W. Hu, Z. Cai, J. Zhu, Q. Ye, F. Ye, Z. Fang, L. Yang, Q. Liang. Crystals **13**, *3*, 410 (2023).
[31] B.A. Rosales, L. Wei, J. Vela. J. Solid State Chem. **271**, 206 (2019).
[32] G. Kresse, M. Marsman, J. Furthmuller. Vienna *ab initio* simulation package. VASP the guide. UniversitätWien, Wien (2018). 233 p.
[33] C. Jacoboni. Theory of Electron Transport in Semiconductors. Springer, Berlin (2010). 588 p.
[34] A. Cantarero, X. Alvarez. In: Nanoscale Thermoelectrics / Eds X. Wang, Zh.M. Wang. Springer, Berlin (2014). P. 141.
[35] S. Ponce, E.M. Margine, C. Verdi, F. Giustino. arXiv:1604.0325[cond-mat.mtrl-sci]
[36] J.-J. Zhou, J. Park, I.-T. Lu, I. Maliyov, X. Tong, M. Bernardi. Comp. Phys. Commun. **264**, 107970 (2021).
[37] B.A. Auld. Acoustic Fields and Waves in Solids. Wiley Intersci. Pub., N.Y. (1973). 411 p.
[38] J.P. Perdew, A. Ruzsinszky, G.I. Csonka, O.A. Vydrov, G.E. Scuseria, L.A. Constantin, X. Zhou, K. Burke. Phys.Rev. Lett. **100**, *13*, 136406 (2008).
[39] T. Baikie, Y. Fang, J.M. Kadro, M. Schreyer, F. Wei, S.G. Mhaisalkar, M. Graetzel, T.J. White. J. Mater. Chem. A **1**, *18*, 5628 (2013).
[40] T.M. Tritt. Thermal Conductivity. Theory, Properties and Applications. Kluver Academic, N.Y. (2004). 290 p.
[41] G.A. Slack, S. Galginaitis. Phys. Rev. **133**, *1A*, A253 (1964).
[42] G.A. Slack. J. Phys. Chem. Solids **34**, *2*, 321 (1973).
[43] G. Slack. Solid State Phys. **34**, 1 (1979).
[44] D. Morelli, G.A. Slack. In: High Thermal Conductivity Materials / Eds S.L. Shindé, J.S. Goela. Springer, Berlin (2006). P. 37.
[45] T. Jia, G. Chen, Y. Zhang. Phys. Rev. B **95**, *15*, 155206 (2017).
[46] C.L. Julian. Phys. Rev. **137**, *1A*, A128 (1965).
[47] O.L. Anderson. J. Phys. Chem. Solids **24**, *7*, 909 (1963).
[48] D. Connétable, O. Thomas. Phys. Rev. B **79**, *9*, 094101 (2009).
[49] A.M.A. Leguy, J.M. Frost, A.P. McMahon, V. Garcia Sakai, W. Kockelmann, C. Law, X. Li, F. Foglia, A. Walsh, B.C. O'Regan, J. Nelson, J.T. Cabral, P.R.F. Barnes. Nature Commun. **6**, *1*, 7124 (2015).
[50] J. Wei, L. Yang, Zh. Ma, P. Song, M. Zhang, J. Ma, F. Yang, X. Wang. J. Mater. Sci. **55**, *27*, 12642 (2020).
[51] X.-L. Shi, X. Tao, J. Zou, Zh.-G. Chen. Adv. Sci. **7**, *7*, 1902923 (2020).
[52] V.P. Zhukov, E.V. Chulkov, FTT **64**, *12*, 1891 (2022). (in Russian).
[53] J.-H. Pöhls, Z. Luo, U. Aydemir, J.-P. Sun, S. Hao, J. He, I.G. Hill, G. Hautier, A. Jain, X. Zeng, C. Wolverton, G.J. Snyder, H. Zhu, M.A. White. J. Mater. Chem. A **6**, *40*, 19502 (2018).
[54] D. Ginting, C.-C. Lin, J.-S. Rhyee. Energies **13**, *1*, 72 (2019).
[55] S.Q. Bai, X.Y. Huang, L.D. Chen, W. Zhang, X.Y. Zhao, Y.F. Zhou. Appl. Phys. A **100**, *4*, 1109 (2010).
[56] A. Togo, L. Chaput, I. Tanaka. Phys. Rev. B **91**, *9*, 094306 (2015).
[57] C. Motta, F. El-Mellouhi, S. Kais, N. Tabet, F. Alharbi, S. Sanvito. Nature Commun. **6**, *1*, 7026 (2015).
[58] Q. Wang, Y. Tang, Z. Horita, S. Iikubo. Mater. Res. Lett. **10**, *8*, 521 (2022).
[59] L. Ma, D. Guo, M. Li, C. Wang, Z. Zhou, X. Zhao, F. Zhang, Z. Ao, Z. Nie. Chem. Mater. **31**, *20*, 8515 (2019).
[60] G.P. Nagabhushana, R. Shivaramaiah, A. Navrotsky. Proc. Nat. Acad. Sci. **113**, *28*, 7719 (2016).

*Translated by Y.Alekseev*